Available online at www.sciencedirect.com
ScienceDirect
Acta Materialia 57 (2009) 3562–3571
Acta MATERIALIA
www.elsevier.com/locate/actamat

Prevalence of shear banding in compression of $Zr_{41}Ti_{14}Cu_{12.5}Ni_{10}Be_{22.5}$ pillars as small as 150 nm in diameter

X.L. Wu [a,*], Y.Z. Guo [b,c], Q. Wei [b,*], W.H. Wang [d]

[a] State Key Laboratory of Nonlinear Mechanics, Institute of Mechanics, Chinese Academy of Sciences, Beijing 100190, China
[b] Department of Mechanical Engineering and Engineering Science, University of North Carolina at Charlotte, Charlotte, NC 28223-0001, USA
[c] School of Aeronautics, Northwestern Polytechnical University, Xi'an, Shaanxi 710072, China
[d] Institute of Physics, Chinese Academy of Sciences, Beijing 100190, China

Received 18 March 2009; accepted 8 April 2009
Available online 6 May 2009

Abstract

Recently, the size dependence of mechanical behaviors, particularly the yield strength and plastic deformation mode, of bulk metallic glasses (BMG) has created a great deal of interest. Contradicting conclusions have been drawn by different research groups, based on various experiments on different BMG systems. Based on in situ compression transmission electron microscopy (TEM) experiments on $Zr_{41}Ti_{14}Cu_{12.5}Ni_{10}Be_{22.5}$ (Vit 1) nanopillars, this paper provides strong evidence that shear banding still prevails at specimen length scales as small as 150 nm in diameter. This is supported by in situ and ex situ images of shear bands, and by the carefully recorded displacement bursts under load control as well as load drops under displacement control. Finite element modeling of the stress state within the pillar shows that the unavoidable geometry constraints accompanying such experiments impart a strong effect on the experimental results, including non-uniform stress distributions and high level hydrostatic pressures. The seemingly improved compressive ductility is believed to be due to such geometry constraints. Observations underscore the notion that the mechanical behavior of metallic glasses, including strength and plastic deformation mode, is size independent at least in Vit 1.

Keywords: Bulk metallic glasses; In situ transmission electron microscopy; Shear banding; Size effect

1. Introduction

Specimen size dependence or the lack thereof in the mechanical properties of bulk metallic glasses (BMG) has received great interest recently [1–7]. Investigations have focused on two aspects: (i) the dependence of yield strength on specimen size [1,5,6,8], paralleling the specimen size effect widely established in crystalline metals [9–11]; (ii) the dependence of plastic deformation mode on specimen size, i.e., whether a plastic flow mode different from macroscopic specimen plasticity operates in miniaturized specimens [1–4,12].

It is a firmly established paradigm that, under mechanical straining, metallic glasses exhibit elastic–perfectly plastic behavior over a wide range of loading conditions at relatively low reduced temperatures with respect to the glass transition temperature [13]. Further, the plastic deformation manifests itself as a consequence of discrete localized shear banding events within extremely narrow regions, only a few tens of nanometer wide. Such characteristics lead to serrated flow if the plastic portion of the stress–strain curve of a BMG specimen is carefully examined [14]. The fundamental reason for such behavior is the lack of dislocations responsible for plastic deformation of crystalline materials. Instead, two entities have been proposed for the understanding of the plastic deformation of BMG: free volumes and shear transformation zones (STZ) [15,16].

* Corresponding authors. Tel.: +86 10 8254 3957 (X.L. Wu); tel.: +1 704 6878213 (Q. Wei).
E-mail addresses: xlwu@imech.ac.cn (X.L. Wu), qwei@uncc.edu (Q. Wei).

1359-6454/$36.00
doi:10.1016/j.actamat.2009.04.013

The objective of this work is to evaluate the plastic deformation behavior of a representative and typical bulk metallic glass, $Zr_{41}Ti_{14}Cu_{12.5}Ni_{10}Be_{22.5}$ (Vit 1), at nanometer scale using in situ compression within a transmission electron microscope. Vit 1 was chosen as the model material for two fundamental reasons. The first is that Vit 1 has been proved to be a very strong glass former and can be easily processed into bulk form at cooling rates as low as 1 K s^{-1} [17], and it shows strong resistance to crystallization in its wide supercooled liquid region. The second reason is that, since its discovery by Peker and co-workers [17], numerous papers have been published on its mechanical behavior over a wide range of loading conditions [18–23]. The specimen size of this work is very close to the theoretically predicted "critical nucleus size" of a shear band (~50–500 nm in diameter) [13,24,25] in BMG based on atomistic simulations.

2. Experimental procedure

$Zr_{41}Ti_{14}Cu_{12.5}Ni_{10}Be_{22.5}$ (Vit 1) BMG ingots were prepared by induction melting pre-mixed powders of the constituent species in an inert gas atmosphere. Measurement via standardized testing of Vit 1 provided the following physical and mechanical data [26]: density (g cm^{-3}) = 5.9; Young's modulus (GPa) = 95; shear modulus (GPa) = 34.1; bulk modulus (GPa) = 114.1; Poisson's ratio = 0.352; yield strength (GPa) = 1.86; glass transition temperature (K) = 618.

Nanopillars for in situ compression experiments were made employing the focused ion beam (FIB) micromachining technique with a very low current (10 nA). Details of the FIB process and associated issues can be found in Ref. [2], where it is pointed out that tapered geometry is almost inevitable when fabricating nanopillars using FIB. This will invite complexity in data processing and quantitative analysis of the experimental results of mechanical testing. Fig. 1 displays a TEM image of a tapered nanopillar fabricated by FIB. Careful measurement shows that the taper angle is ~15° (the taper angle is defined as the angle between the pillar axis and the side). Another set of nanopillars have ~10° taper angles (to be shown later).

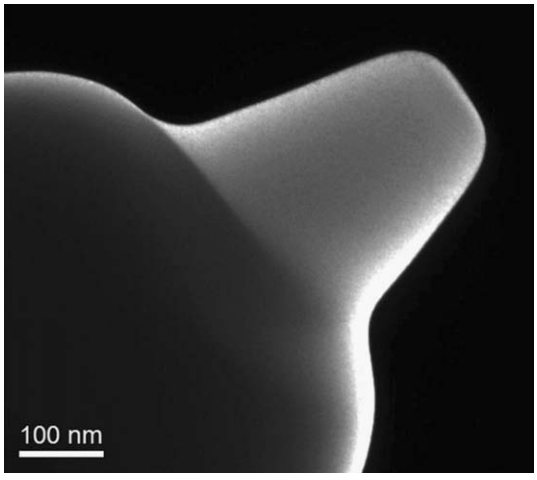

Fig. 1. Image of a tapered nanopillar of Vit 1 fabricated by FIB. This is Sample I. Details about the geometry and dimension of this sample are to be found in the text.

In situ nano-compression experiments were carried out at room temperature in a JEOL 3010 transmission electron microscope operating at 300 kV, using a Hysitron TEM PicoIndenter employing a miniature actuatable capacitive transducer equipped with a flat-end diamond punch. This in situ indentation system allows a mechanical load to be applied accurately and the resultant vertical displacement to be measured. It can also be operated in displacement control mode. In addition, a piezoelectric actuator is available for fine-scale positioning of the transducer and/or punch relative to the pillar.

Two sets of samples with similar geometry and dimensions are examined in detail. The first set of samples have a taper angle ~15°, with the TEM image shown in Fig. 1. The pillar top diameter is ~75 nm; the pillar bottom diameter is ~286 nm; the diameter at medium height is ~220 nm, and the pillar height is ~262 nm. It should be noted that the top and side faces of the pillar are connected by an arc with a radius of curvature ~50 nm. The second set of samples have a taper angle ~10°. The pillar top diameter is ~100 nm, the pillar bottom diameter is ~320 nm, the diameter at medium height is ~276 nm, and the pillar height is ~420 nm. The connecting arc between the top and side faces of the pillar also has a radius of curvature ~50 nm. Both sets of pillars are fabricated out of the bulk sample, and therefore the base material is also Vit 1. It is worth noting that, as the pillar diameters are much larger than the penetration depth (10 nm) of the Ga ions used in the FIB cutting, implantation damage, if any, that may lead to artifacts will be negligible [27]. The two sets of amorphous samples, hereafter referred to as Sample I and Sample II, were compressed in the transmission electron microscope under an open-loop mode of load control and displacement control (10 nm s^{-1} for 10 s of increasing displacement), respectively. The in situ compression experiments were videotaped at a rate of 30 frames s^{-1}. The load frame recorded the load–displacement history of the specimens. Beam-heating effects are regarded as minimal, as the nanopillars are part of a much larger BMG piece in contact with a flat diamond punch of high thermal conductivity.

After in situ compression within the transmission electron microscope, some nanopillars were examined by scanning electron microscopy (SEM) for evidence (or the lack thereof) of shear bands.

3. Experimental results

Fig. 2A:a–f are representative dark-field (DF) TEM images taken from sample I in the course of in situ nano-compression. Such DF images are actually snapshots extracted from a video recorded during a load–controlled nano-compression test. Owing to the taper geometry of

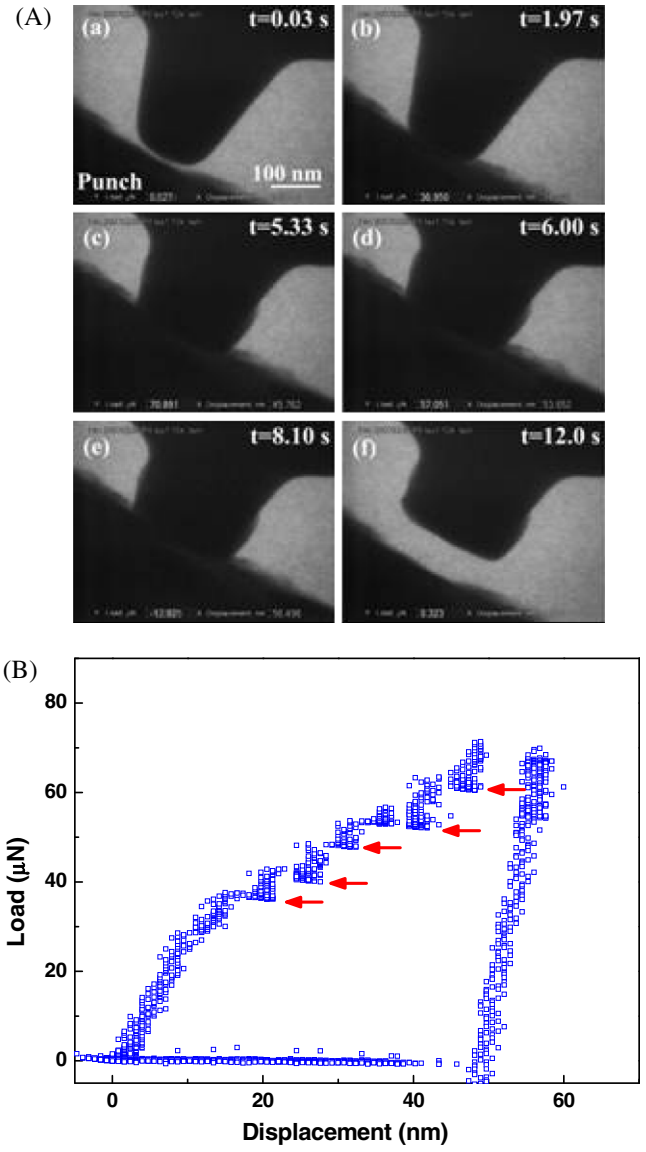

Fig. 2. (A) Snapshots of in situ TEM compression of a Vit 1 metallic glass pillar (Sample I). The different stages of the nano-compression are depicted by individual still frames (a–f) at different times. Frame of $t = 0.03$ s corresponds to the initial stage of the test. All frames are extracted from a dynamic video sequence. Evidence of shear offset starts to appear in frame (c). (B) The recorded load–displacement curve corresponding to snapshots series in (A). Arrows point to the displacement burst events. While the TEM images fail to reveal all the displacement burst events, the load–displacement curve has clearly captured the major events. The first displacement burst occurs upon depressing ~16 nm from the top, which is translated into a nominal strain of 0.06.

FIB-fabricated nanopillar, the plastic deformation starts from the pillar top in contact with the pressing diamond flat punch. No evidence of localized shearing can be observed until frame c, where an obvious shear offset starts to emerge. In other words, the top half of the Vit 1 nanopillar might have flowed to a large strain in a uniform manner before localized shearing kicked in. While DF TEM images may not be able to reveal the distinct individual shearing events during nano-compression, the recorded load–displacement displayed in Fig. 2B does provide very valuable information on such events. A series of displacement burst events have been marked by arrows in the load–displacement curve corresponding to Sample I. The first burst occurs after the diamond punch has pushed down ~16 nm. This displacement corresponds to a nominal strain of ~0.06 if the nominal height of 262 nm is used for this nanopillar. Note that this nominal strain is much larger than the "elastic strain limit" of Vit 1 (~0.02 from standardized measurement [23,26,28,29]). Also note that, based on detailed imaging and diffraction analyses of the compressed Vit 1 nanopillar throughout, no apparent crystallization, global or local, has been observed. It has been further noticed that the plastic deformation of the nanopillar was not limited on a single shear plane. Instead, V-shaped inter-crossing shear events are recorded, as shown in (Fig. 2A:d–f). This becomes more evident in the bright-field post-loading TEM image displayed in Fig. 3 where multiple shear bands are present.

Similar behavior is more or less repeatedly captured in all nanopillars of Vit 1 studied in this work. As yet another example, Fig. 4A:a–f presents a series of DF TEM images extracted from Sample II during an in situ nano-compression experiment. This time, the nano-compression was performed in a displacement–control mode. The first shear offset is observed in frame 4A:b, after considerable shortening in pillar length. Fig. 4B displays the associated load–displacement plot of this sample. Profuse load dips or load drops are marked by arrows, which supposedly correspond to shear banding events. The first load dip occurs after the diamond punch depressed the nanopillar to ~40 nm from its original top position. If the nominal height of this pillar is taken to be ~420 nm, the nominal strain at which the first load drop occurs is ~0.095, which again is much larger than the "elastic strain limit" recorded for Vit 1 via conventional methods.

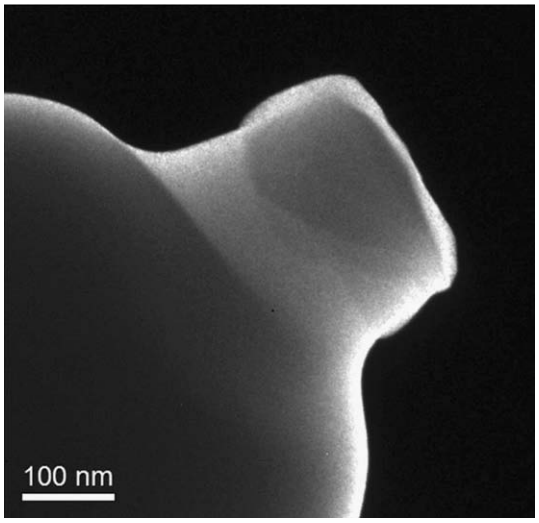

Fig. 3. Bright-field TEM image of the compressed Sample I. Multiple shear bands are revealed which are typically observed in bulk BMG samples.

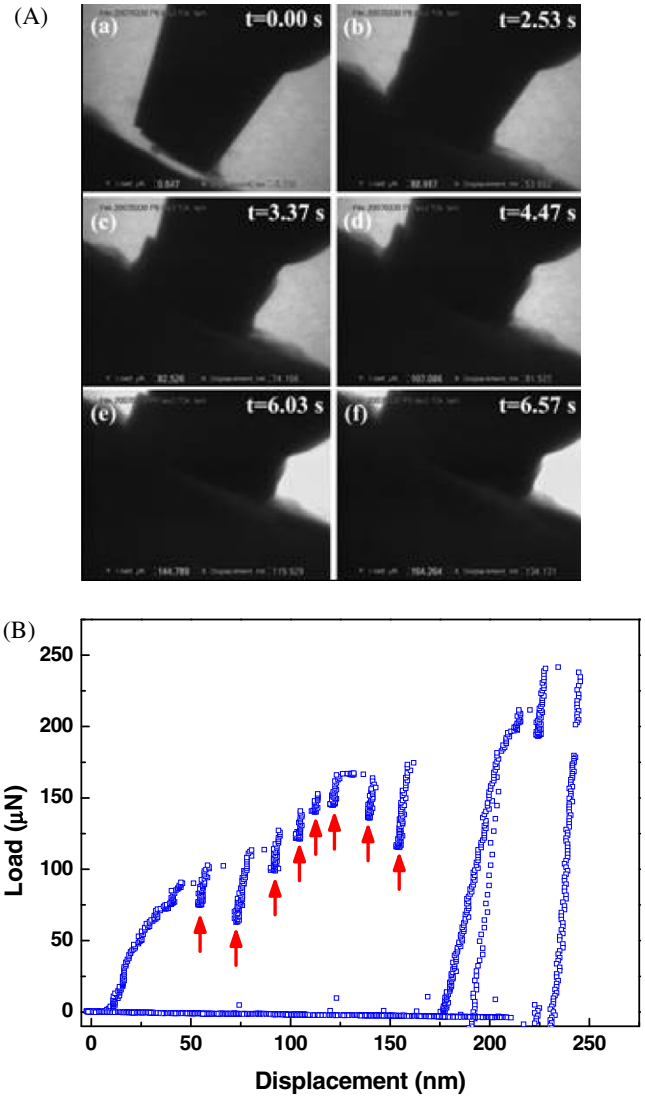

Fig. 4. (A) Snapshots of in situ TEM compression of a Vit 1 metallic glass pillar (Sample II). The different stages of the nano-compression are depicted by individual still frames (a–f) at different times. The frame of $t = 0.00$ s corresponds to the initial stage of the test (before the diamond punch pushes the nanopillar). All frames are extracted from a dynamic video sequence. Evidence of shear offset starts to appear in frame (b). The experiment was performed under displacement–control. (B) The recorded load–displacement curve corresponding to snapshots series in (A). Arrows point to the dips or load drops in the load–displacement curve which are presumably due to shear banding events. The first load drop occurs upon depressing ~40 nm from the top, which is translated into a nominal strain of 0.095. See text for detailed descriptions.

The snapshots from live TEM video clearly suggest that the pillar experienced obvious shortening, along with an increase in diameter. In this case, a major shear banding event did set in. It should be noted that, here, the pillar was first pressed lightly, and then the load was removed. Upon reloading, a "shear band" was initiated. This relatively large shear band has run across the entire sample, causing a shear step on the side (Fig. 4A:b). A film that clearly shows the progression of this shear step has been successfully recorded (not shown here). With continued loading, a major portion of the subsequent deformation occurred at the same location, as seen in snapshots in (Fig. 4A:b–e). However, the reduction in sample height and increase in lateral dimensions cannot be fully accounted for by the strain, owing to the growth of this single shear offset alone. In other words, there appears to be a homogeneous flow in the sample in addition to the advance of the offset itself, as well as initiation and development of secondary shear bands, as evidenced by the many subsequent load dips in the load–displacement curve (Fig. 4B).

The primary shear offset that was initiated in frame b grows slowly, even when the total nominal overall axial strain of the pillar has reached 21%. Surprisingly, this process has not led to the rapid shear rupture which has been frequently observed in macroscopic MG samples under standardized uniaxial compression. The sample absorbed much of the plastic work, including that from the repeated shear banding events. Serrations are obvious in the load–displacement curve in Fig. 4B. The load drops in the curve, and the jerky advancement of the shear step seen in the recorded movie show a one-to-one correspondence. Close inspection reveals that the shear displacement rate in each jerky motion is only a small fraction of ~1 μs, releasing energy in a stepped and controlled fashion, which is different from macroscopic samples. In the latter case, the shear displacement avalanche driven by the large accumulated energy runs like a crack, at a rate of ~10.0 mm μs^{-1}, up to the speed of sound.

The final example is provided in Fig. 5 from Sample I. The bright-field TEM snapshots show the deformation process of the nanopillar in a load–control experiment. It is shown that the first piece of evidence for shear banding appears quite early (Fig. 5A:b); the associated load–displacement curve is displayed in Fig. 5B. It is observed that the first displacement burst occurs upon depressing to ~8 nm from the punch/pillar contact, which is translated into a nominal strain of ~0.028. This nominal strain is still larger than the "elastic strain limit" reported for Vit 1. Supposedly before the first displacement burst, the pillar is undergoing uniform plastic deformation. Post-loading image (Fig. 5C) indicates multiple shear bands, presumably originating from the pillar top, in accordance with the load–displacement curve where a number of displacement bursts have been observed.

Note that in all the Vit 1 nanopillars tested, no "catastrophic" fracture was observed. There was also no apparent change in contrast due to crystallization throughout the in situ TEM DF observation, even in the offset regions near the edges of the nanopillars, which are very thin and might have been heavily deformed. This is also supported by inspecting the electron diffraction patterns and post-deformation still images (not shown). Bright nanometer-scale crystals were seen in the DF images only when the diamond punch was repeatedly tapping the asperities on the contact surface, presumably causing friction and local heating. Therefore, the enhanced plasticity observed here comes entirely from the flow of the monolithic glass, which is very

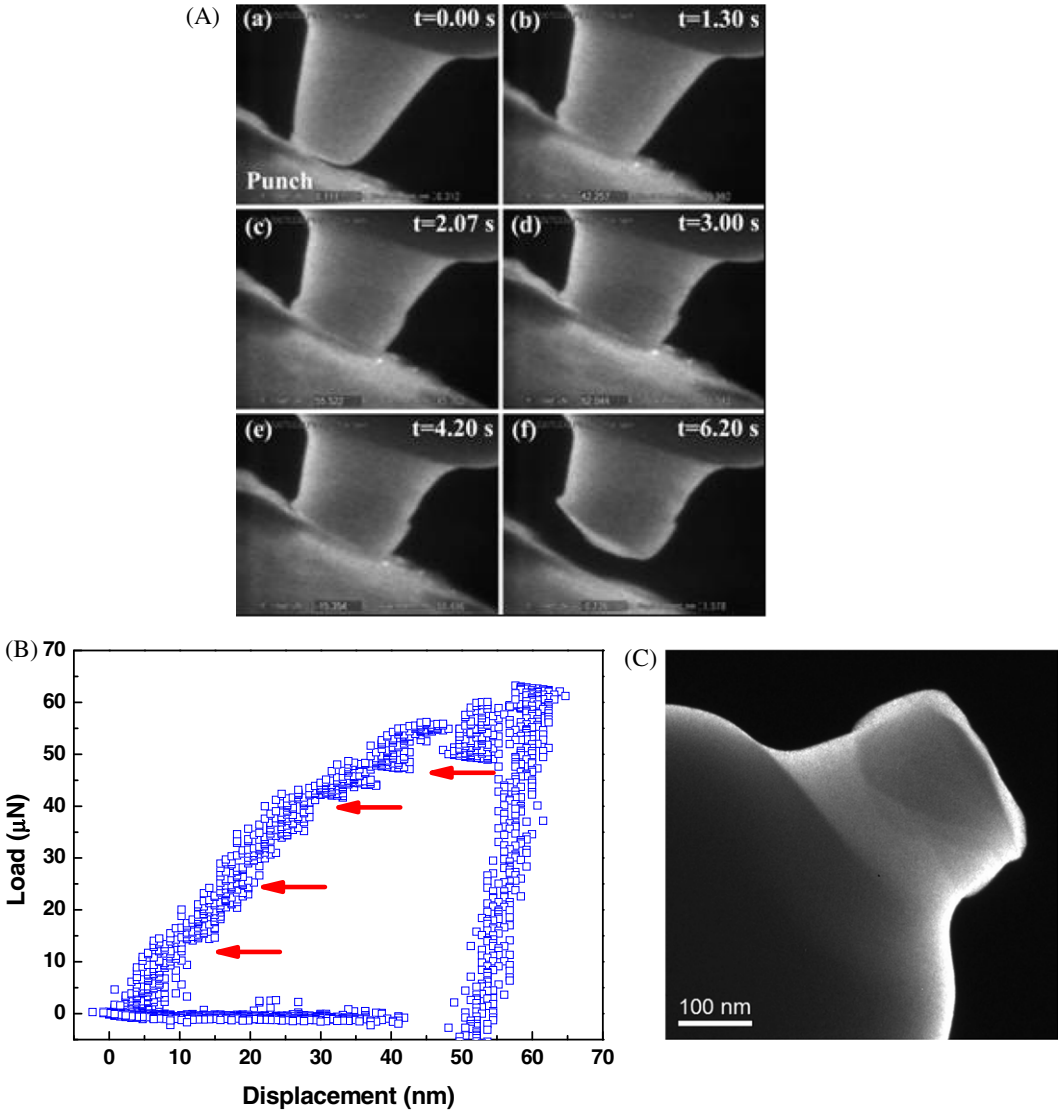

Fig. 5. (A) Bright-field snapshots of in situ TEM compression of a Vit 1 metallic glass pillar (Sample I). The different stages of the nano-compression are depicted by individual still frames (a–f) at different times. The frame of $t = 0.00$ s corresponds to the initial stage of the test (before the diamond punch pushes the nanopillar). All frames are extracted from a dynamic video sequence. Clear evidence of shear offset starts to appear in frame (c). The experiment was performed under load control. (B) The recorded load–displacement curve corresponding to snapshots series in (A). Arrows point to the displacement bursts which are presumably due to shear banding events. The first load drop occurs upon depressing only ~8 nm from the top, which is translated into a nominal strain of 0.028. See text for detailed descriptions. (C) The post-loading BF TEM image showing multiple shear bands apparently originated from the top of the pillar.

different from the deflection and branching of shear bands due to precipitation of nano-crystalline phases, as observed in some MG [30,31], and from the microcracking and crack-branching of brittle materials [32].

In summary, in situ compression experiments of nanopillars of Vit 1 show that shear banding is still operational. In load control mode, shear banding events manifest themselves as displacement bursts in the load–displacement curves; in displacement control mode, they manifest themselves as load drops in the load–displacement curves. Multiple shear banding events have been observed in all the experiments. Unlike experimental observations of free-standing samples in conventional standardized mechanical testing where "catastrophic" shear failure is exclusively present, no such phenomenon has been observed in the nanopillars. It was also observed that the nominal strain before the first shear band kicks in is much larger than the "elastic strain limit" reported for Vit 1, implying that significant "uniform" plastic deformation has occurred before localized shear banding events took over. The significance of such observations will be discussed in the following section.

4. Discussion

This section presents in-depth discussions on the in situ nano-compression results of Vit 1 nanopillars from this work. It focuses on the following aspects. First, the defor-

mation and failure mode of the nanopillars of Vit 1 are discussed based on the experimental observations. Then the yield strength of the Vit 1 nanopillars as derived from the load–displacement curves as well as image analysis is elaborated upon. Finite element modeling is used to examine the stress state within the nanopillars.

4.1. Plastic deformation of Vit 1 nanopillars

It should first be pointed out that the deformation mode of the Vit 1 nanopillars in this work is quite different from bulk, macroscopic samples under standard uniaxial compression where friction between the loading faces of the specimen and compression platens is usually carefully eliminated by means of lubrication. One should also keep in mind that, in conventional uniaxial compression, the specimen geometry meets the major criteria such that the experimental results should faithfully reflect the intrinsic behavior of the material under investigation. The present in situ compression experiments of nanopillars of Vit 1 are far from such ideal conditions. The following major factors are of primary concern when interpreting and understanding the experimental observations. First, the nanopillars all have tapered geometry, with significant taper angles (15° and 10° for Sample I and II, respectively). As Zhang and co-workers found through detailed finite element modeling (FEM) [33], such geometry results in artificial or spurious strain hardening even for elastic–perfect plastic materials. From a mechanics point of view, the apparent strain hardening due to such geometry effect will at least delay plastic instability such as localized shear banding [34]. This factor should partly contribute to the observed nominal strain before the first localized shear banding event, which is much larger than the reported "elastic strain limit" of Vit 1. Second, unlike conventional uniaxial compression of bulk samples, the top surface of the nanopillar is in direct contact with the diamond punch, i.e., no lubricant is applied between them. What is more, the pillar is sitting on its base of the same material with a significant fillet curvature radius. (See Fig. 1 for Sample I. Sample II is similar in this respect.) This, according to the careful FEM analysis of Zhang and co-workers [33], also helps to delay plastic as well as elastic instability (buckling).

Another factor which has largely been neglected in previous efforts in nano-/micro-compression of metallic glasses as well as crystalline materials is the geometry of the top of the pillar. As Fig. 1 shows, nanopillars of Vit 1 fabricated by FIB in this work have curved tops. That is, the side of the nanopillar and the top surface are connected by an arc surface with a curvature radius in the amount of ~50 nm. The effect of this configuration has not been considered in the work of Zhang et al. [33], nor has it been addressed in the more recent work of Schuster et al. [2] and Yang et al. [35]. This should not be of great concern for relatively large pillars whereby the curved connection only accounts for a small portion of the whole specimen. However, this should no longer be the case for nanopillar, as shown clearly in Fig. 1. Schuster and co-workers performed FEM on tapered posts in order to examine the distribution of shear stresses in the post as a function of taper angle [2]. Their results show that the non-uniformity of shear stress increases significantly with the taper angle. Such strong stress gradient associated with relatively large taper angle will naturally render analyzing experimental results more involved. If the curved connecting part between the pillar top and the side is taken into account, especially for nanopillars, the stress gradient effect will be more significant. This is particularly true in the initial stage of in situ compression.

To evaluate both the effect of the taper angle and the top geometry on the experimental results, particularly the stress and strain distributions within the pillar, the authors also performed FEM. To simulate the problem best, a 3-D model was constructed which maps the taper angle and pillar top geometry according to the actual parameters associated with Sample I and Sample II of this work. It concentrates on the geometry effects and the stress/strain distributions within the pillars before shear banding. Both elastic ($E = 95$ GPa, $\nu = 0.352$ [17]) and elastic–perfectly plastic ($\sigma_y = 1.86$ GPa [26]) cases were considered and compared with experimental results. Two element types (i.e., C3D4, a 4-node linear tetrahedron; and C3D8R, an 8-node linear brick, reduced integration, hourglass control) were used which can provide more accurate results on the top of the pillar, while keeping the overall calculation cost low. Fig. 6 depicts the model that has been created (corresponding to Sample I, Fig. 1).

A friction coefficient of 0.1 is applied between the diamond punch and the Vit 1 pillar top, and the pillar *per se* is sitting on the base of the same material with no interface

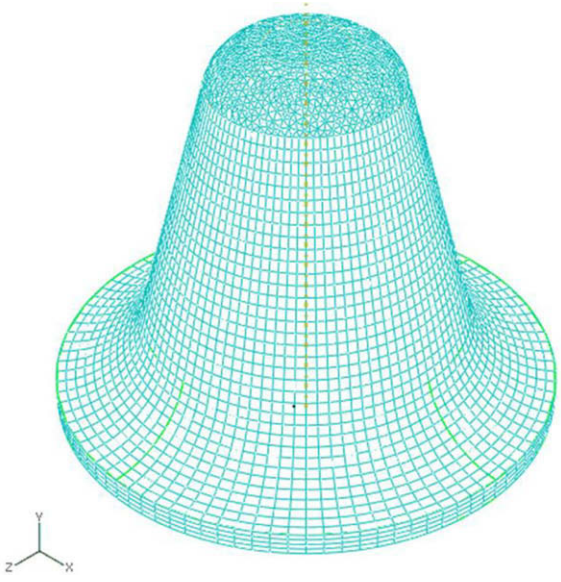

Fig. 6. FEM model for the examination of the effects of geometry constraints on the stress state of the nanopillars. This particular model is for the simulations of the behaviors of Sample I.

between them. A commercial FEM package (ABAQUS) was used for the simulations. Fig. 7 displays representative FEM results showing stress distributions within pillars of different taper angle and top geometry. It is seen that straight pillars have relatively uniform stress distribution. However, with increasing taper angle, the von Mises stress becomes less uniformly distributed. This scenario is exacerbated by the presence of a curved connection between the top surface and the side wall of the pillar.

The most striking characteristic, the authors believe, is the evolution of hydrostatic pressure within the pillar due to the geometry constraints accompanying such experiments. Hydrostatic pressure as high as >2.0 GPa has been observed in certain locations of the pillar near the pillar top. Fig. 8 shows the evolution of hydrostatic pressure within the pillar as a function of the applied load. The effects of taper angle and pillar top geometry were examined. The figure shows that the maximum hydrostatic pressure increases drastically with increased taper; the curved top geometry also contributes significantly to the hydrostatic pressure. A maximum hydrostatic pressure of >1 GPa is easily achieved within the pillar as the load exceeds 5 μN, far below the load corresponding to the major shear banding event (the first displacement burst in the load–displacement curve). While in a very recent paper, Kiener and co-workers [36] mention that multiple-axial stress state may exist in the pillars during micro-compression experiments, no quantitative estimation has been provided. It will be seen later that the presence of such high hydrostatic pressure has a profound impact on the mechanical behavior of BMG as observed in nano-/micro-compression.

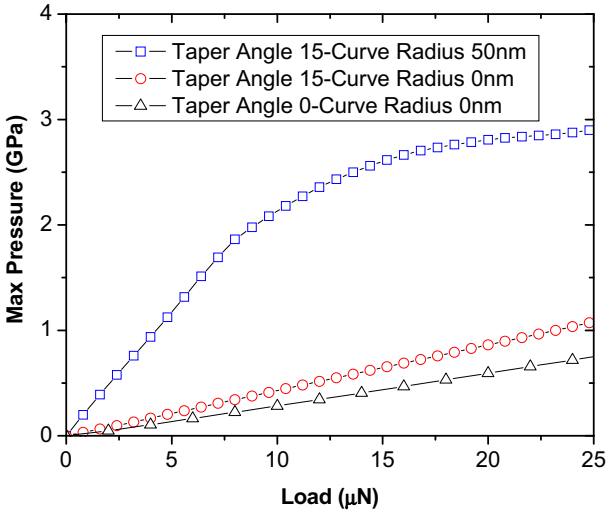

Fig. 8. Evolution of hydrostatic pressure within the pillar with load. Both effects of taper angle and pillar top geometry were examined. It shows that the curvature radius of the part connecting the top and the side of the pillar has a substantial effect on the maximum hydrostatic pressure within the pillar.

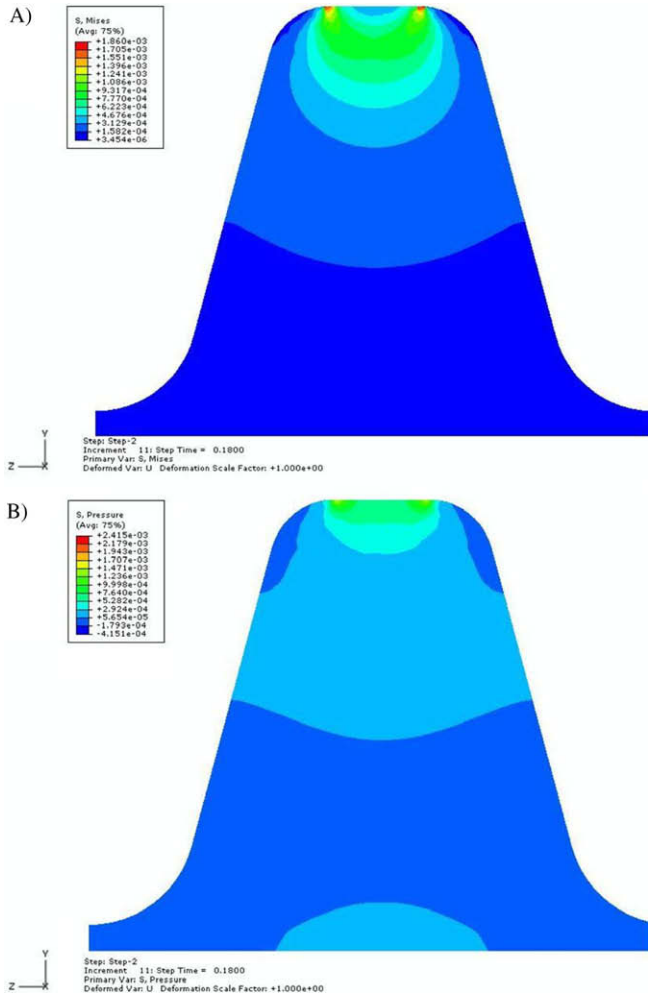

Fig. 7. Distribution of von Mises stress (A) and hydrostatic pressure (B) in Sample I. Relevant parameters used to build up the model: 15° taper angle, 50 nm top curvature radius. Units of von Mises stress and pressure, 1000 GPa; current load, 7.2 μN; top cross-section radius, 35 nm.

Prolonged "uniform" plastic deformation or even "super plasticity" has recently been reported for BMG [3,4,37,38]. But it is a well-known fact that BMG are devoid of any ductility under uniaxial tension, even though a very recent report does provide evidence of necking and tensile plasticity in very small specimens during in situ TEM experiments [12]. It has also been observed that the capability of metallic glasses to exhibit plastic deformation under compression strongly depends on test conditions such as sample geometry (aspect ratio), stress concentrations, and hydrostatic pressure [37,39–44]. For example, Jiang and co-workers [43] and Zhang and co-workers [44] report strong dependence of compressive ductility (or malleability) on specimen aspect ratio of a Zr-based bulk metallic glass, i.e., compressive strain to failure increases with decreasing specimen aspect ratio (length/diameter). Lewandowski and co-worker found that imposed hydrostatic pressure does not have significant effect on the strength of Vit 1, but it does increase compressive strain to failure [41]. It was also observed that imposing a pressure on the metallic glass before loading leads to considerable improvement in compressive ductility [45].

Notwithstanding the experimental results, a plausible theory is still lacking to explain such phenomena. FEM shows that various levels of hydrostatic pressure indeed exist beneath the pillar top (Fig. 7). The authors therefore believe that the improved compressive ductility or the delayed shear banding initiation of the Vit 1 nanopillars is a direct consequence of the geometry constraints which lead to the build-up of hydrostatic pressure that suppresses or at least retards shear banding events.

An alternative way of looking at the pressure sensitivity of the strength of BMG has been taken by Ramamurty and co-workers [46,47]. It appears that the classical Tabor equation, i.e., $H = C\cdot\sigma_y$ that links the hardness and compressive yield strength of a material is closely obeyed with $C \simeq 3.0$ if the material is pressure insensitive. Most crystalline metals fall into this category [48]. When the parameter C is bigger than 3.0, it suggests pressure dependence of the yield strength. Values of C close to 4.0 have been observed for Vit 1 [46], indicating its strong pressure dependence. In that sense, C is also called the "plastic constraint factor" [46]. Taking this into account, it is then even more involved to get a clear picture of the yield stress of Vit 1 nanopillars.

From a mechanics point of view, the intrinsic ductility of a viscoplastic material depends on two major factors: decent capability of strain hardening according to the simple Considère criterion [49] and decent strain rate sensitivity (SRS), which depicts the dependence of materials' mechanical behavior on loading rate [49,50]. SRS helps suppress or retard growth of plastic inhomogeneities, as demonstrated by the classical analysis of Hart [51], and later dealt with by Lin and co-workers [52]. It appears that both stabilizing factors for homogeneous plasticity are absent in BMG. Moreover, vanishing or even negative SRS values have been reported for Vit 1 and other BMG [18,53–57]. It then transpires that BMG should be strongly susceptible to plastic instability such as localized shear banding. Geometry constraints such as exist in the nanopillar compression of this work do delay the shear banding events, but they fail to eliminate the shear banding mechanism completely, the sole conceivable mechanism available for plastic deformation of BMG at relatively low reduced temperatures. The extent of discrete shear events in the amorphous pillars here is small, and a large number of them are closely spaced in a small volume over a total displacement distance of only ~100 nm. This renders the appearance of the plastic flow nearly "homogeneous". Thus, the plastic deformation is "homogeneous" in the sense that, much as in crystalline metals, plastic flow carriers are active everywhere, even though they themselves are discrete.

Recent efforts have identified a close link between the toughness and "intrinsic plasticity" of BMG with the elastic properties such as shear modulus (G)/bulk modulus (K) ratio and Poisson's ratio (ν) [58–60]. It has long been found that, for crystalline metals, a lower G/K ratio or higher ν leads to better ductility [61]. Close examination on the effects of G/K ratio and ν on the ductility of a material shows that it is the stress condition under a given applied load in the crack tip that depends on these parameters, which in turn leads to ductile or brittle behavior of the material [61]. It is thus inferred that the seemingly improved ductility in the nanopillars of Vit 1 can also be understood in a similar way.

4.2. Yield strengths of Vit 1 nanopillars

A few articles have reported that the yield strength of BMG increases with decreased specimen size [5,6]. Huang and co-workers [7] observed that smaller samples have improved ductility (or more accurately, malleability) and lower yield strength, and attributed the results to the faster cooling rates experienced by small samples during preparation of the amorphous alloy. The sample sizes were, however, in the millimeter range.

To evaluate the yield strengths of the Vit 1 nanopillars of this study, first the yield strength is defined as the stress at which the first displacement burst appears in the load–control experiment, or the stress at which the first load drop occurs in the displacement–control experiment. With this in mind, it is still not straightforward as to how to calculate the stresses corresponding to those events. Since it appears that the shear band is always initiated from the top of the nanopillar, it should be reasonable to use the stress close to the pillar top. However, the top is constantly moving, and the top surface area is evolving during compression of the pillar. Therefore, some assumptions have to be made for the calculation of the top surface area. Here, it was observed that the first shear banding events occur after the diamond punch has depressed the nanopillar to various displacements (Figs. 2B, 4B and 5B). For example, the first displacement burst in Fig. 2B (Sample I) appears after the diamond punch has depressed the nanopillar top to ~16 nm, and the associated load is ~36 μN. To calculate the stress corresponding to this shear banding event, the cross section of the nanopillar at 16 nm downward from the pillar top is used, which is carefully measured to be ~169 nm (diameter). Thus the compressive stress is ~1.611 GPa. This value is smaller than the widely reported compressive yield strength of Vit 1 (~1.89 GPa). Therefore, here the phenomenon of "the smaller, the stronger" was not observed.

If similar calculation of "yield strength" is performed for Sample II (Fig. 4), a stress value of 1.99 GPa associated with the first load drop of the load–displacement curve is obtained. This value is slightly above the bulk yield strength of Vit 1. Such diverse values of "yield strength" can hardly be understood on any physics grounds. As shown in the work of Schuster et al. [1,8] scattering of "yield strength" measurements becomes more profound with decreased pillar size. The authors would rather regard this to be from the dramatically changed stress state within the pillar due to geometry constraints. In other words, the complex stress state within the pillar during nano-compression renders it very difficult to derive the "yield stress"

associated with each pillar based on the load–displacement data. If an elastic–perfectly plastic constitutive behavior is used to perform FEM, one can see that the load–displacement curve of the tapered pillar with curved top geometry follows the experimental results quite faithfully (Fig. 9). It also asserts that the spurious strain hardening is due to the taper geometry as the input is for elastic–perfectly plastic material. However, if a constant top surface is assumed and is used to calculate the stress of the pillar, the stress corresponding to the first displacement burst turns out to be ~9.0 GPa, more than four times the bulk yield stress of Vit 1. Therefore, it is intriguing but challenging to examine the specimen size effect on the yield strength of metallic glasses using nano-/micro-compression experiments. However, a rationale is lacking in anticipating such effects in metallic glasses, owing to the absence of any operators that provide the strengthening mechanisms, as dislocations do in crystalline metals.

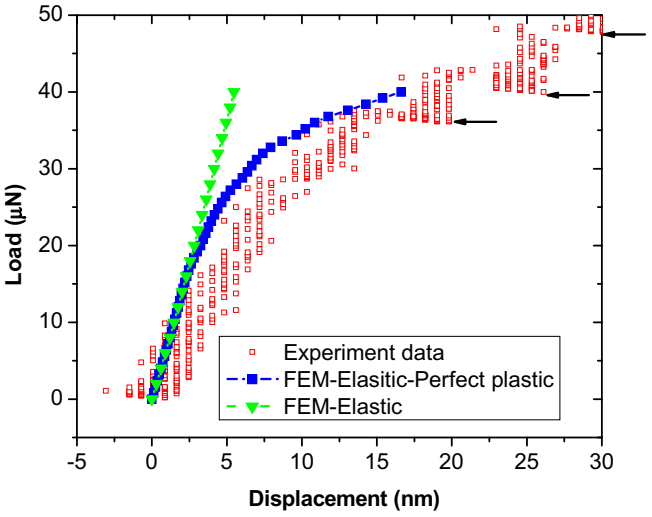

Fig. 9. Comparison of simulated load–displacement curves vs the experimental data. It shows that the simulated curve based on an elastic–perfectly plastic constitutive model does trace the experimental data faithfully.

Fig. 10 displays two post-mortem SEM images of Vit 1 nanopillars. A primary shear band is observed in Fig. 10a, and multiple shear bands can be observed in Fig. 10b. Furthermore, the nanopillar in Fig. 10b has considerably sheared with respect to its base. The preponderance of such evidence, as well as other results presented earlier, suggests that shear banding is still the prevalent deformation mechanism in nanopillars of Vit 1. The fact that "catastrophic" failure did not occur may merely be a consequence of the geometry constraints in such experiments.

Finally, it should be pointed out that, obtaining unequivocal evaluation of the size effect of metallic glasses may best be performed on free-standing pillars. With the recent advent of the nano-molding technique [62,63], free-standing pillars of BMG may be available in the near future. Fewer geometry constraints will be anticipated if micro-/nano-compression experiments can be performed on such free-standing pillars, and consequently, the interpretation of the experimental results will be more straightforward.

5. Summary and concluding remarks

The mechanical responses of Vit 1 pillars with nominal diameters as small as 150 nm were examined using in situ micro-/nano-compression within a transmission electron microscope. The major findings are summarized as follows.

Load–displacement curves show clear evidence of displacement bursts in the load–control mode and load drops in the displacement–control mode. Such displacement bursts/load drops correspond well to the shear banding events as revealed by in situ TEM video frames. Both in situ and ex situ examination of the Vit 1 nanopillars suggests that shear banding is still the predominant plastic deformation mode at such small length scales.

Detailed finite-element analyses indicate that the geometry constraints intrinsic to such nano-/micro-compression experiments render very complex stress states within the pillar. In particular, a non-uniform stress distribution has been observed in the pillars. What is more, a great amount

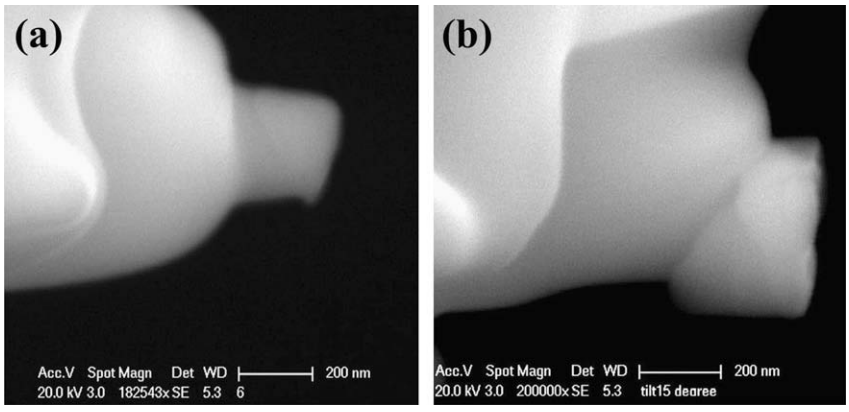

Fig. 10. (a) Post-mortem SEM micrographs showing the presence of localized shear bands formed during the compression experiments. In (b), multiple shear bands are present, and the pillar has been sheared significantly with respect to its base.

of hydrostatic pressure is built up within the pillar, with its maximum value easily exceeding 1 GPa. The seemingly improved malleability is believed to be largely due to the dramatically changed stress state within the nanopillars as compared with conventional standardized compression experiments.

Acknowledgments

X.L. Wu thanks Dr. Z.W. Shan, Hysitron Inc., for the assistance with the in situ TEM and for many fruitful discussions. X.L. Wu was supported by NSFC Nos. 50890171, 10721202 and 50571110, CAS No. KJCX2-YW-M04 and MOST No. 2004CB619305. Y.Z. Guo would like to thank the Ph.D. Student Fund of the Chinese Ministry of Education (Contract No. 20070699044) and the 111 Project of PR China (Contract No. B07050) for financial support. He would also like to thank the China Scholarship Council (Contract No. [2007] 3020) for financial support.

References

[1] Schuster BE, Wei Q, Ervin MH, Hruszkewycz S, Miller MK, Hufnagel TC, et al. Scripta Mater 2007;57:517.
[2] Schuster BE, Wei Q, Hufnagel TC, Ramesh KT. Acta Mater 2008;56:5091.
[3] Shan ZW, Li J, Cheng YQ, Minor AM, Asif SAS, Warren OL, et al. Phys Rev B 2008;77:155419.
[4] Volkert CA, Donohue A, Spaepen F. J Appl Phys 2008;103:083539.
[5] Lee CJ, Huang JC, Nieh TG. Appl Phys Lett 2007;91:161913.
[6] Lai YH, Lee CJ, Cheng YT, Chou HS, Chen HM, Du XH, et al. Scripta Mater 2008;58:890.
[7] Huang YJ, Shen J, Sun JF. Appl Phys Lett 2007;90:081919.
[8] Schuster BE. Micro-Pillar Compression of Nanocrystalline and Amorphous Metals. Mechanical Engineering, vol. Ph.D. Baltimore: The Johns Hopkins University, 2008. p.186.
[9] Uchic MD, Dimiduk DM, Florando JN, Nix WD. Science 2004;305:986.
[10] Greer JR, Oliver WC, Nix WD. Acta Mater 2005;53:1821.
[11] Volkert CA, Lilleodden E. Philos Mag 2006;86:5567.
[12] Guo H, Yan PF, Wang YB, Tan J, Zhang ZF, Sui ML, et al. Nature Mater 2007;6:735.
[13] Schuh CA, Hufnagel TC, Ramamurty U. Acta Mater 2007;55:4067.
[14] Chen HS. Scripta Metall 1973;7:931.
[15] Falk ML. Phys Rev B 1999;60:7062.
[16] Falk ML, Langer JS. Phys Rev E 1998;57:7192.
[17] Peker A, Johnson WL. Appl Phys Lett 1993;63:2342.
[18] Lu J, Ravichandran G, Johnson WL. Acta Mater 2003;51:3429.
[19] Wright WJ, Schwarz RB, Nix WD. Mater Sci Eng A 2001;319–321:229.
[20] Jiang MQ, Ling Z, Meng JX, Dai LH. Philos Mag 2008;88:407.
[21] Raghavan R, Murali P, Ramamurty U. Intermetallics 2006;14:1051.
[22] Murali P, Ramamurty U. Acta Mater 2005;53:1467.
[23] Bruck HA, Christman T, Rosakis AJ, Johnson WL. Scripta Metall Mater 1994;30:429.
[24] Schuh CA, Lund AC, Nieh TG. Acta Mater 2004;52:5879.
[25] Li QK, Li M. Appl Phys Lett 2007;91:231905.
[26] Johnson WL, Samwer K. A Phys Rev Lett 2005;95:195501.
[27] Bei H, Shim S, Miller MK, Pharr GM, George EP. Appl Phys Lett 2007;91:111915.
[28] Zhang Y, Zhao DQ, Wang RJ, Wang WH. Acta Mater 2003;51:1971.
[29] Lu J, Ravichandran G, Johnson WL. Acta Mater 2001;51:3429.
[30] Fan C, Ott RT, Hufnagel TC. Appl Phys Lett 2002;81:1020.
[31] Hufnagel TC, Fan C, Ott RT, Li J, Brennan S. Intermetallics 2002;10:1163.
[32] Lutz EH, Claussen N, Swain MV. J Am Ceram Soc 1991;74:11.
[33] Zhang H, Schuster BE, Wei Q, Ramesh KT. Scripta Mater 2006;64:181.
[34] Wright TW. The physics and mathematics of adiabatic shear bands. Cambridge: Cambridge University Press; 2002.
[35] Yang Y, Ye JC, Lu J, Liu FX, Liaw PK. Acta Mater 2008;57:1613.
[36] Kiener D, Motz C, Dehm G. Mater Sci Eng A 2009;505:79.
[37] Wu FF, Zhang ZF, Mao SX. J Mater Res 2007;22:501.
[38] Liu YH, Wang G, Wang RJ, Zhao DQ, Pan MX, Wang WH. Science 2007;315:1385.
[39] Liu CT, Heatherly L, Easton DS, Carmichael CA, Schneibel JH, Chen CH, et al. Metall Mater Trans A 1998;29:1811.
[40] Sunny G, Lewandowski J, Prakash V. J Mater Res 2007;22:389.
[41] Lewandowski JJ, Lowhaphandu P. Philos Mag A 2002;82:3427.
[42] Wu WF, Li Y, Schuh CA. Philos Mag 2008;88:71.
[43] Jiang WH, Fan FJ, Choo H, Liaw PK. Mater Lett 2006;60:3537.
[44] Zhang ZF, Zhang H, Pan XF, Das J, Eckert J. Philos Mag Lett 2005;85:513.
[45] Yu P, Bai HY, Zhao JG, Jin CQ, Wang WH. Appl Phys Lett 2007;90:051906.
[46] Patnaik MNM, Narasimhan R, Ramamurty U. Acta Mater 2004;52:3335.
[47] Keryvin V, Prasad KE, Gueguen Y, Sanglebauf J-C, Ramamurty U. Philos Mag 2008;88:1773.
[48] Tabor D. The hardness of metals. Oxford: Clarendon Press; 1951.
[49] Hart EW. Acta Metall 1970;18:599.
[50] Bai Y, Dodd B. Adiabatic shear localization. Oxford: Pergamon Press; 1992.
[51] Hart EW. Acta Metall 1967;15:351.
[52] Lin IH, Hirth JP, Hart EW. Acta Metall 1981;29:819.
[53] Hufnagel TC, Jiao T, Li Y, Xing LQ, Ramesh KT. J Mater Res 2002;17:1441.
[54] Bruck HA, Rosakis AJ, Johnson WL. J Mater Res 1996;11:503.
[55] Dubach A, Torre FHD, Loffler JF. Philos Mag Lett 2007;87:695.
[56] Li H, Subhash G, Gao XL, Kecskes LJ, Dowding RJ. Scripta Mater 2003;49:1087.
[57] Sunny G, Yuan FP, Prakash V, Lewandowski J. Appl Phys Lett 2008;104:093522.
[58] Lewandowski JJ, Wang WH, Greer AL. Philos Mag Lett 2005;85:77.
[59] Poon SJ, Zhu AW, Shiflet GJ. Appl Phys Lett 2008;92:261902.
[60] Na JH, Park ES, Kim YC, Fleury E, Kim WT, Kim DH. J Mater Res 2008:23 523.
[61] Kelly A, Tyson WR, Cottrell AH. Philos Mag 1967;15:567.
[62] Kumar G, Tang HX, Schroers J. Nature 2009;457:868.
[63] Schroers J. JOM 2005;57:35.